JOURNAL OF GEOPHYSICAL RESEARCH, VOL. 104, NO. D24, PAGES 31,411–31,419, DECEMBER 27, 1999

Cloud liquid water, mean droplet radius, and number density measurements using a Raman lidar

David N. Whiteman

Laser Remote Sensing Branch, NASA Goddard Space Flight Center, Greenbelt, Maryland

S. Harvey Melfi

Department of Physics, University of Maryland, Baltimore County, Baltimore

Abstract. A new technique for measuring cloud liquid water, mean droplet radius, and droplet number density is outlined. The technique is based on simultaneously measuring Raman and Mie scattering from cloud liquid droplets using a Raman lidar. Laboratory experiments on liquid microspheres have shown that the intensity of Raman scattering is proportional to the amount of liquid present in the spheres. This fact is used as a constraint on calculated Mie intensity assuming a gamma function particle size distribution. The resulting retrieval technique is shown to give stable solutions with no false minima. It is tested using Raman lidar data where the liquid water signal was seen as an enhancement to the water vapor signal. The general relationship of retrieved average radius and number density is consistent with traditional cloud physics models. Sensitivity to the assumed maximum cloud liquid water amount and the water vapor mixing ratio calibration are tested. Improvements to the technique are suggested.

1. Introduction

Because of the great radiative impact of clouds and the difficulty associated with modeling them, cloud research is a central part of such programs as the Department of Energy's Atmospheric Radiation Measurements (ARM) program [*Stokes and Schwartz*, 1994] and the World Meteorological Organization (WMO) World Climate Research Program's (WCRP) International Satellite Cloud Climatology Project (ISCCP) [*Rossow and Schiffer*, 1999]. Accurate in situ and remote measurements of cloud properties are needed to help validate model predictions and satellite observations. The remote ground-based techniques that are currently in use for determining cloud liquid water and droplet size generally rely on complex inversion algorithms to derive the desired quantities using a combination of instruments including radar [*Dong et al*., 1997]. Radars are well known to be insensitive to the smallest droplets located near the bottoms of clouds [*Clothiaux et al*., 1999]. We report here on progress toward developing a technique for remotely determining cloud liquid water content, average droplet size, and droplet number density using Raman lidar. This technique has the advantage of being most sensitive in the lower portion of the cloud where radar-based techniques have difficulty.

2. Background

Raman lidar systems have been used for many years to measure various atmospheric parameters including water vapor and aerosols [*Melfi*, 1972; *Whiteman et al*., 1992; *Goldsmith et al*., 1998]. The measurement of water vapor is typically made by centering a band-pass filter at the first Raman vibrational transition ν_1 of 3657 cm^{-1}. However, the Raman spectrum from liquid water spans a range of ~2800–3800 cm^{-1} and thus overlaps this region of the spectrum [*Whiteman et al*., 1999]. This means that if any liquid water is present in the volume that is being sensed by a Raman lidar, the signal measured in the water vapor channel will be increased because of Raman scattering from the liquid.

This effect has been observed in clouds using the NASA Goddard Space Flight Center Scanning Raman Lidar (SRL) [*Melfi et al*., 1997]. Here we present a technique which allows liquid water content, average droplet radius, and droplet number density to be simultaneously determined from these measurements. We then test the technique using Raman lidar data and suggest improvements in the measurement technique.

3. Theory: Raman Scattering From Spheres

Laboratory measurements of Raman spectra from levitated microspheres have been performed by numerous investigators [*Vehring et al*., 1995, 1998; *Schweiger*, 1991; *Buehler et al*., 1991; *Bazile and Stepowski*, 1994; *Vehring*, 1998]. These experiments have been performed over various size parameter ranges, where size parameter is defined as the circumference of the sphere divided by the input wavelength. The size ranges in these studies were: 20–120 [*Vehring et al*., 1998], 60–120 [*Schweiger*, 1991], 120–240 [*Vehring et al*., 1995], 160–400 [*Buehler et al*., 1991], and 1700–4500 [*Bazile and Stepowski*, 1994]. For an input laser wavelength of 351 nm, the corresponding droplet radii are approximately 1.1–6.7 μm, 3–6.7 μm, 6.7–13.4 μm, 8.9–22.4 μm, and 95–250 μm, respectively. These studies have revealed that Raman spectra of spheres possess many resonances. The number of resonances in the Raman spectrum can exceed the number of resonances in the corresponding Mie spectrum since boundary conditions must be met for 2 wavelengths in the former case. However, all of the laboratory studies have found that by integrating over a range of sizes and thus through numerous resonances, the intensity of Raman scattering is proportional to the total vol-

Paper number 1999JD901004.
0148-0227/99/1999JD901004$09.00

ume of the droplets. In addition, the size parameter range of 1–30 (0.06–1.7 μm) has been studied by computer simulation [*Vehring et al*., 1998]. This study revealed that except for size parameters below 3 ($\sim$0.2 μm), the same proportionality between the intensity of Raman scattering from a droplet and the droplet volume held true.

Nonprecipitating liquid water droplets in clouds are nearly perfect spheres [*Pruppacher and Klett*, 1997] with radii ranging between approximately 0.5 and 50 μm depending on cloud type, with most droplet radii being smaller than 25–30 μm. Thus the experiments on Raman scattering from droplets mentioned above have investigated essentially the entire size range of real cloud droplets. It is reasonable to expect that the linearity between Raman intensity and cloud droplet volume will hold for the relatively small range of cloud droplet sizes not yet studied (G. Schweiger, personal communication, 1998). Thus after calibration a measurement of Raman scattering from liquid water in a cloud will yield the liquid water content of a cloud volume directly. The lidar system used to make the measurements analyzed here will now be described.

4. Lidar Description

The NASA/GSFC Scanning Raman Lidar is housed in a single mobile trailer and has participated in numerous field campaigns since its first deployment in 1991. The system has received several modifications since that time and now contains two lasers for optimized performance during either nighttime or daytime. For nighttime operations a Lambda Physik LPX240iCC excimer laser is used. A XeF gas mixture is used, resulting in an output wavelength of 351 nm. We operate the laser at a repetition rate of 400 Hz with a pulse energy of 30–60 mJ depending on the experiment objective. This yields an output power of 12–24 W. These output power levels can be maintained for up to 12 hours before a gas change is required.

Laser light scattered by molecules and aerosols produces an intense return at the laser wavelength. In addition, molecules such as water vapor, nitrogen, and oxygen produce much weaker return signals because of Raman scattering which are at wavelengths shifted from the laser wavelength. The return wavelengths for water vapor, nitrogen, and oxygen are approximately 403, 382, and 371 nm, respectively. All four of these signals are collected by a 0.76 m, F/5.2 (F number is defined as effective focal length divided by the primary aperture of telescope system), variable field-of-view (0.5–2.5 mrad) Dall-Kirkham telescope manufactured by Starr Optical. The telescope is mounted horizontally on a 3.7 m optical table and aligned with a large (1.2 m $\times$ 0.8 m) flat scan mirror which is also mounted on the optical table.

The telescope output is collimated and then split among eight photomultiplier tubes (PMT) using dichroic beam splitters and interference filters from Barr Associates. There are two PMTs used to detect each wavelength. One PMT receives a small portion of the signal intensity and is used for the low-altitude returns below $\sim$4 km while the second PMT receives the remainder of the signal and is used for the high-altitude returns above $\sim$3 km. Hamamatsu 1398 PMTs are used for the excimer-based measurements.

During fair weather operations the optical table slides through an opening in the back of the trailer, deploying the scan mirror to the outside. This provides a 180° horizon to horizon scan capability. Using the motorized scan mirror, atmospheric profiles can be acquired at any angle in a single plane perpendicular to the trailer or continuously scanned from horizon to horizon. In addition, the trailer has three windows installed which allow all-weather operations to occur. These windows allow measurements to be obtained vertically as well as at small angles above the horizontal in either direction. Measurements near the horizon are used to improve vertical resolution in the boundary layer.

Table 1. Scanning Raman Lidar Optical Channel Configuration

	Center Wavelength, nm	FWHM, nm
XeF (351.1 nm)		
aerosol	352.4	6.1
oxygen (1550 cm^{-1})	371.2	6.8
nitrogen (2330 cm^{-1})	383.2	8.0
water vapor (3657 cm^{-1})	403.9	8.6
Nd:YAG (354.7 nm)		
aerosol	354.8	0.3
oxygen	375.4	0.3
nitrogen	386.7	0.3
water vapor	407.4	0.25

The center wavelengths and bandwidths are shown for measurements based on both lasers in use in the system: a XeF excimer laser and a frequency-tripled neodymium:yttrium/aluminium/garnet (Nd:YAG) laser. FWHM, full width at half maximum.

To facilitate daytime measurements of water vapor and aerosols, the SRL uses a custom Continuum neodymium:yttrium/aluminium/garnet (Nd:YAG) laser, narrowband interference filters, and a dual field-of-view optics design. The laser contains frequency-tripling optics and transmits 300 mJ pulses of 354.7 nm light at 30 Hz, yielding an average power of 9 W. The laser beam divergence is reduced to below 0.2 mrad by means of a $\times$3 beam expander. This low divergence permits the use of a narrow (0.25 mrad) field of view in addition to the wide (2.0 mrad) field of view. The narrow field of view, coupled with the use of narrowband (0.2–0.3 nm band-pass) interference filters, reduces the background skylight and therefore increases the signal-to-noise ratio during daytime operations. As in the case of the excimer-based measurements, data are acquired at the laser wavelength as well as at the Raman-shifted wavelengths for water vapor, nitrogen, and oxygen molecules using two PMTs for each wavelength. In this case those wavelengths are approximately 408, 387, and 375 nm, respectively. The PMTs used for these measurements are EMI 9214.

Each PMT is amplified using a Phillips Scientific model 6950 ($\times$10) amplifier, discriminated using Phillips Scientific model 708 (300 MHz) discriminators, and then finally counted using Computer Automated Measurement and Control (CAMAC)–based DSP Technology model 2090/4101 (100 MHz) scalars. The scalars are clocked using a Santa Fe Energy Research Synchron-II clock pulse generator. Data are recorded as 1 min profiles which correspond to the accumulation of signals from $\sim$23,000 laser shots when using the excimer laser. The photon-counting data have a range resolution of 75 m. National Instruments LabView software running on a PC controls the data acquisition, monitors system performance, and is also used to display real-time images of the evolution of both water vapor and aerosols.

Table 1 shows the center wavelengths of each channel and the widths of the filters used for measurements with the XeF excimer and Nd:YAG lasers. Notice that the widths of the

filters used with the excimer-based measurements are particularly broad. This is due to the three-line nature of the output spectrum of the XeF laser [*Whiteman et al*., 1993]. Because of this, the broad water vapor filter transmits a significant portion of the liquid water spectrum. Figure 1 shows the spectral trace of the water vapor filter overlaid on Raman spectra for bulk liquid water scattering at several temperatures [*Whiteman et al*., 1999]. For reference, the band origin of the ν_1 transition in water vapor is at 3657 cm^{-1}, and the width of the ν_1 feature is $\sim$20 cm^{-1}. (Because of the three lines of the XeF laser the lidar return signals actually consist of three bands which are separated by $\sim$100 cm^{-1}. Only the liquid water spectra relating to the central, most intense band are shown in Figure 1. Future work will focus on making liquid water measurements using the Nd:YAG, which possesses a much narrower spectral output.)

The first SRL measurements of liquid water were discovered as an enhancement of the water vapor signal in clouds [*Melfi et al*., 1997]. Those measurements have been further analyzed here under the assumption that the component of the combined water vapor plus liquid water mixing ratio signal which exceeds saturation is proportional to the liquid water mixing ratio. To retrieve droplet size and number density, both the liquid water content and the backscatter coefficient of the cloud are required. The liquid water content is directly proportional to the Raman intensity as described in section 3. Calculation of the backscatter coefficient from the lidar data and the droplet size retrieval technique will now be described.

5. Lidar Backscatter Coefficient From a Cloud

The Raman lidar routinely measures aerosol backscattering ratio as a function of range in the atmosphere. This ratio can be defined as

$$R_A = \frac{I_{\text{ray}} + I_{\text{mie}}}{I_{\text{ray}}},$$

and it is calculated from the lidar data using

$$R_A = k\,\frac{O_A(z)}{O_N(z)}\,\frac{I_A}{I_N}\,\Delta\tau(\lambda_0,\,\lambda_N,\,z),$$

where all the quantities except the proportionality constant k are a function of height. I_{ray} and I_{mie} are the Rayleigh and Mie backscatter intensities, respectively, and I_A and I_N are the lidar aerosol channel and lidar nitrogen channel intensities, respectively. $O_A(z)$ and $O_N(z)$ are the overlap functions pertaining to the aerosol and nitrogen channels, respectively. The ratio $O_A(z)/O_N(z)$ is essentially unity for the data analyzed here. The quantity $\Delta\tau(\lambda_0, \lambda_N, z)$ is the differential transmission due to the fact that the aerosol and nitrogen signals make their return trip from the scattering volume to the lidar at different wavelengths. Thus the round-trip extinction due to molecules will be different for these two wavelengths. Since atmospheric absorption is negligible at these wavelengths, the differential extinction is corrected first by calculating the differential Rayleigh scattering at the two wavelengths. This calculation requires a knowledge of the atmospheric density which is usually obtained from a radiosonde but also can be obtained from an atmospheric model. The round-trip extinction due to aerosols is usually different as well. It is estimated for aerosols by using the aerosol signal intensity measured by the lidar [*Whiteman et al*., 1992]. For the heights of the clouds analyzed here, the differential transmission correction amounted to less than $\sim$2%.

After correction for differential transmission the constant of proportionality k is then established by normalizing the ratio of the lidar signals to unity in a region of the atmosphere that is essentially free of aerosol scattering at the laser wavelength. This normalization region is typically between 6 and 10 km [*Russell et al*., 1982].

The aerosol backscatter coefficient can now be calculated from the aerosol backscattering ratio using the Rayleigh differential backscatter cross section for the mixture of atmospheric gases below 100 km, which is given by [*Measures*, 1984]

$$\sigma_{\text{ray}} = 5.45(550/\lambda)^4\ 10^{-28}\ \text{cm}^2\ \text{sr}^{-1}$$

$$\beta_{\text{ray}} = N_{\text{mol}}\sigma\ \text{cm}^{-1}\ \text{sr}^{-1},$$

where σ_{ray} is the Rayleigh differential backscattering cross section, N_{mol} is the molecular number density obtained either from a model or from a radiosonde measurement, λ is the laser wavelength in nanometers, and β_{ray} is the Rayleigh backscatter coefficient. Using these formulas, the cloud backscatter coefficient β_{cloud} is determined as a function of height in the cloud simply by

$$\beta_{\text{cloud}} = \beta_{\text{ray}}(R_A - 1). \tag{1}$$

6. Cloud Droplet Size Distribution

Following *Pruppacher and Klett* [1997], a unimodal cloud droplet size distribution can be approximated reasonably well by a gamma distribution:

$$n(a) = Aa^{\beta}\exp\,(-Ba^{\gamma}).$$

Choosing $\gamma = 1$ and $\beta = 2$ yields the empirically determined Khrgian-Mazin distribution, which has been shown to be a good approximation for single-maximum droplet size distributions found in real clouds [*Khrgian*, 1963]. The new distribution function

$$n(a) = Aa^2\exp\,(-Ba)$$

becomes

$$n(a) = \frac{27}{2}\,\frac{N}{\bar{a}^3}\,a^2\exp\left(-3\,\frac{a}{\bar{a}}\right) \tag{2}$$

when normalization considerations for total droplet number and average radius are applied. Here $n(a)\,da$ is the number of drops per cm^3 with radii in the range of $(a, a + da)$, N is the total number of drops per cm^3, and $\bar{a}$ is the average radius.

The definition of cloud liquid water content

$$w_L(\text{g m}^{-3}) = 10^6\left(\frac{4\pi}{3}\right)\rho_w\int_0^{\infty} a^3 n(a)\,da,$$

reflects the fact that real cloud liquid water contents are on the order of 10^{-6} g cm^{-3}. In this expression, ρ_w is the density of water in g cm^{-3}. Since

$$\int_0^{\infty} a^3 n(a)\,da = \frac{27}{2}\,\frac{N}{\bar{a}^3}\int_0^{\infty} a^5\exp\left(-3\,\frac{a}{\bar{a}}\right)\,da = \frac{20N}{9}\,\bar{a}^3,$$

the following result is obtained:

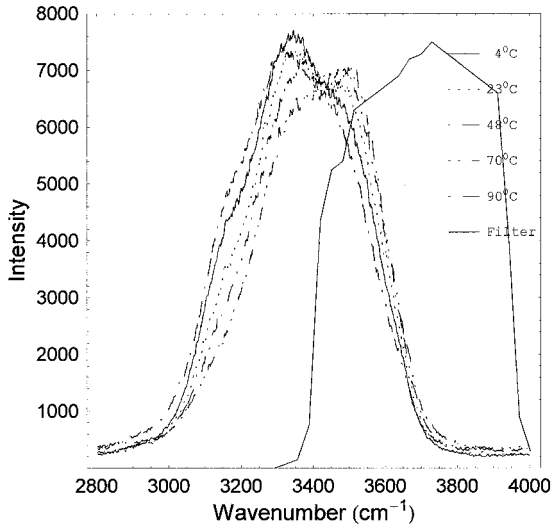

Figure 1. The transmission of the water vapor filter used for the XeF-based measurements along with spectral traces of Raman scattered intensity from liquid water as a function of wavenumber at several temperatures. The Raman liquid water measurements are from *Whiteman et al*. [1999]. The band origin of the ν_1 transition in water vapor is at 3657 cm^{-1}. The ν_1 transition has a width of ~20 cm^{-1}.

$$N = \frac{27}{80\pi}\, 10^{-6}\, \frac{w_L}{\rho_w \bar{a}^3}. \tag{3}$$

At this point the outline for the algorithm to extract liquid water, average droplet radius, and total droplet number density can be seen. Equation (3) offers a constraint on $\bar{a}^3 N$ once the liquid water content of a particular cloud volume is known. The Raman lidar requires a calibration to provide w_L, but, given that calibration, the value of the product $\bar{a}^3 N$ is known. The simultaneously measured Rayleigh plus Mie signal from the lidar can then be used to provide an additional constraint on the problem since Mie scattering theory can be used to calculate the expected backscatter intensity from the cloud.

7. Cloud Backscatter Intensity Modeling Using Mie Scattering

The normalized differential backscatter cross section for spherical water droplets was computed using a commercially available package [*Barber and Hill*, 1990]. The index of refraction for pure water at 351.1 nm [*Irvine and Pollack*, 1968] was used. The computation was performed for droplet size parameters x (defined as the wave vector times the radius, which equals the circumference divided by the wavelength) ranging from 1 to 1800, which, for an input wavelength of 351.1 nm, corresponds to droplet radii ranging from approximately 0.06 to 100 μm. This covers the droplet size ranges found in most clouds. The step size of $0.02x$ used in the calculation corresponds to ~0.001 μm and reveals many fine resonances as shown in Figure 2. However, it is possible that resonances that occur at much finer resolution could contribute significantly to the Mie backscatter cross section. This will be studied in the future using techniques such as complex angular momentum (CAM) theory which allow resonances to be quickly located [*Guimaraes and Nussenzveig*, 1994].

To calculate the anticipated backscatter intensity from a distribution of cloud droplets, the normalized differential backscattering cross section is converted to actual differential backscatter cross section $d\sigma(\pi, a)/d\Omega$ by multiplying by the cross-sectional area. If the size distribution is known, the backscatter coefficient of a cloud volume element is then given by

$$\beta_{\text{cloud}} = \int_0^\infty n(a)\, \frac{d\sigma}{d\Omega}(\pi, a)\, da,$$

which, using the Khrgian-Mazin distribution for $n(a)$ from (2) and the expression for β_{cloud} from (1), becomes

$$\beta_{\text{ray}}(R_A - 1) = \frac{27}{2}\, \frac{N}{\bar{a}^3} \int_0^\infty a^2 \exp\left(-3\, \frac{a}{\bar{a}}\right) \frac{d\sigma}{d\Omega}(\pi, a)\, da. \tag{4}$$

As an example, the integrand in (4) is shown in Figure 3 for the case $N = 100$ cm^{-3} and $\bar{a} = 10$ μm where the Mie differential backscatter cross section has been summed to 0.1 μm resolution.

The retrieval technique consists of simultaneously solving (3) and (4). However, using (3), N may be eliminated from (4), which yields the following equation in the single unknown $\bar{a}$, the average radius:

$$\beta_{\text{ray}}(R_A - 1) = \frac{729}{160\pi}\, \frac{10^{-6}}{\bar{a}^6}\, \frac{w_L}{\rho_w} \int_0^\infty a^2 \exp\left(-3\, \frac{a}{\bar{a}}\right) \frac{d\sigma}{d\Omega}(\pi, a)\, da. \tag{5}$$

This equation must be solved as a function of range in the cloud. Once the average radius is determined at each range, the droplet number density is determined using (3). The form

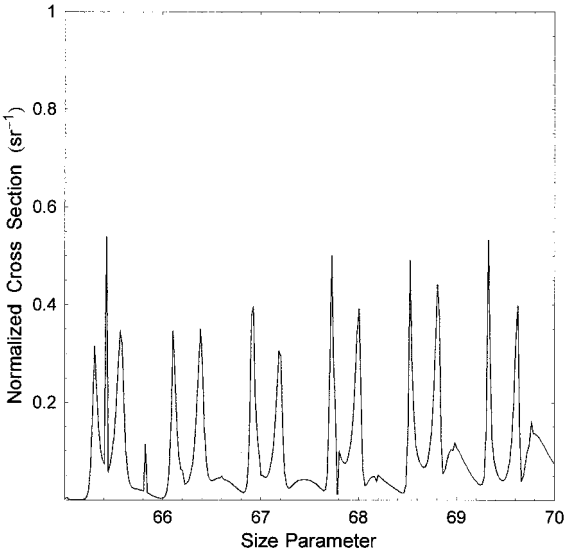

Figure 2. Normalized differential backscattering cross section for a size parameter range of 65–70. Many resonances are visible using a step size of $0.02x$ (corresponding to 0.001 μm). The normalized cross section is the actual cross section divided by the cross-sectional area of the particle. This plot covers a range of droplet radii of ~3.7–4.0 μm for an input wavelength of 351.1 nm.

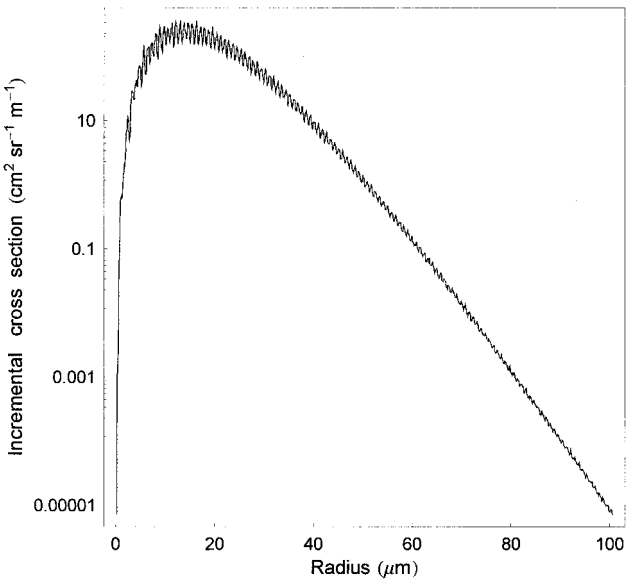

Figure 3. The product of the size distribution and the backscatter cross section for the case of droplet number density of 100 cm^{-3} and average droplet radius of 10 μm. This is the integrand in equation (4).

of this equation depends on the assumed droplet size distribution. The dependence of the retrieved values on this distribution will be tested in the future.

8. Analysis

8.1. Stability of Solution

To test the robustness of the retrieval equations outlined in sections 5–7, the stability of the solution of (5) was tested for several test cases. One of those is shown in Figure 4. Using typical values of cloud backscatter coefficient (km^{-1} sr^{-1}) and liquid water content (g m^{-3}) of 1 and 0.1, respectively, the solution for average droplet radius was found to be ~4.7 μm. Figure 4 shows the difference between the right- and left-hand sides of (5) as a function of average radius. The solution at 4.7 μm is a stable minimum. The technique was tested using cases which covered a large range of combinations of liquid water content and aerosol backscatter coefficient. In all cases the solution was found to be a stable minimum.

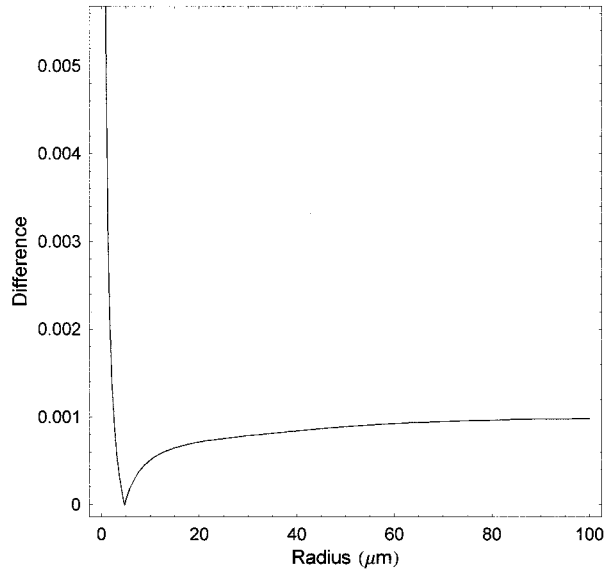

Figure 4. Function space of equation (5) for the solution of average radius given cloud backscatter coefficient and liquid water content. The retrievals showed a stable minimum for all cases tested.

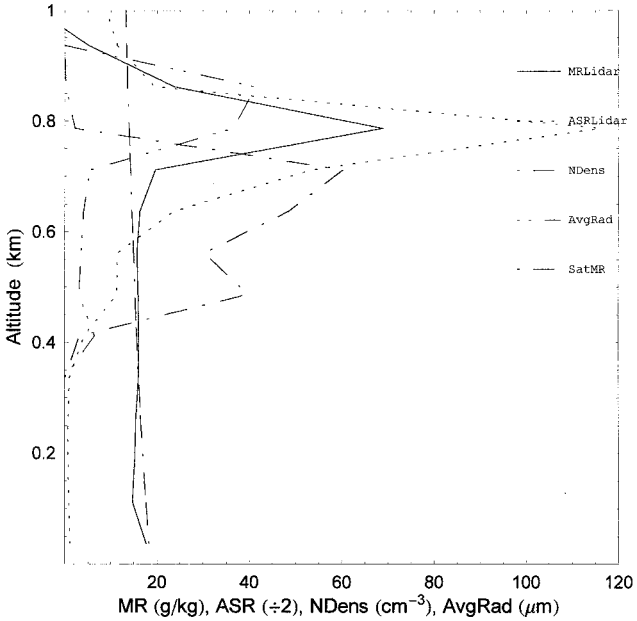

Figure 5. Lidar-derived water vapor mixing ratio (MRLidar), cloud backscatter ratio (ASRLidar), cloud droplet number density (NDens), and average droplet radius (AvgRad) based on data from Wallops Flight Facility on September 9, 1995. Also shown is the saturation mixing ratio (SatMR) from a radiosonde measurement. The portion of the water vapor signal that is in excess of saturation is taken to be proportional to the liquid water content. Average droplet radius is retrieved by assuming a maximum liquid water content in the cloud of 1 g m^{-3}. Average droplet radius varies from approximately 3 to 40 μm, and particle number densities range from 1 to 60 cm^{-3}. The retrievals show the general relationship of the droplets growing in size moving upward in the cloud. Also, the number density remains roughly constant through the lower part of the cloud but then abruptly decreases at the top of the cloud. This relationship between droplet radius and number density agrees with cloud models. These are the same water vapor and aerosol data as were shown in Figure 7 of *Melfi et al*. [1997].

8.2. Analysis of Earlier SRL Data

As a preliminary test of the cloud retrieval routines outlined in sections 5–7, SRL data from the Second Convection and Moisture Experiment (CAMEX2) held at Wallops Flight Facility in 1995 were analyzed. On the night of September 9, strong enhancements of the water vapor signal were measured in clouds which were due to Raman scattering from the liquid droplets in the cloud [*Melfi et al*., 1997]. These strong enhancements are shown in Figure 5 as the curve labeled "MRLidar." This is the lidar water vapor mixing ratio signal which shows mixing ratios in excess of saturation ("SatMR") between the altitudes of approximately 0.35 and 0.9 km. The assumption was made that the portion of this signal in excess of saturation was due to liquid water scattering and thus was proportional to

the liquid water content of the cloud. The liquid water curve was thus obtained by subtracting the saturation profile from the liquid plus vapor profile. This was then converted to units of liquid water content by assuming that the maximum liquid water content of the cloud was 1 g m^{-3} for this cloud, which had an optical depth approximately equal to 3.0. We chose this approach as a way to test our retrieval technique and not as an absolute calibration of the lidar. Also shown are the strong elastic return from the cloud, the retrieved average radius, and the corresponding number density.

It is generally believed that above cloud base, where essentially all condensation nuclei have become droplets, the droplet number density will remain relatively constant until coalescence and collisions toward the top of the cloud cause the average radius to increase and the number density to decrease [*Rogers and Yau*, 1989]. The retrieved values from the lidar show these relationships. Between 0.4 and 0.7 km the retrieved radii are in the range of ~3–6 μm with the number densities typically between 40×10^6 and 60×10^6 m^{-3}. Above 0.7 km the retrieved radii rise to ~40 μm while the number densities fall to a level of ~$1–2 \times 10^6$ m^{-3}.

The retrieved radii and number densities below 0.7 km are considered to be quite reasonable on the basis of extensive measurements made in marine cumulus clouds [*Khrgian*, 1963]. However, the values of average droplet radius and droplet number density retrieved above 0.7 km are rather large and small, respectively, based on these same measurements. However, recent measurements have shown that large droplets of radii >40–50 μm may actually exist in the majority of nonprecipitating clouds [*Wiscombe et al*., 1984]. In addition, scanning radiometer measurements of optical thickness and effective droplet radius in marine stratocumulus have shown that the location of the largest droplets is highly correlated with the regions of the cloud having lowest optical thickness [*Nakajima et al*., 1991]. Therefore, while 40 μm seems a rather large value for the average radius of the distribution, it is not unreasonable that droplets of this size could exist in a nonprecipitating cloud. There are several sources of error in the retrieval technique which could also influence the retrieved values. They will be considered now.

8.3. Sensitivity to Maximum Liquid Water Content and Water Vapor Mixing Ratio Calibration

The lidar has not yet been calibrated for liquid water scattering. For this reason the maximum liquid water content was chosen on the basis of a knowledge of typical values in clouds. The value chosen for maximum liquid water content influences the values retrieved for droplet size and number density. In addition, the amount of supersaturation that is present in the combined water vapor plus liquid water profile is determined by both the lidar water vapor mixing ratio calibration and by the temperature profile from the radiosonde which gives the saturation mixing ratio. The sensitivity of the retrievals to both the assumed maximum liquid content and to the water vapor mixing ratio calibration will now be tested. The sensitivity to temperature from the radiosonde is similar to that due to mixing ratio calibration.

The final calibration number that was applied to all the SRL water vapor mixing ratio data acquired at CAMEX2 was determined through a statistical analysis of all intercomparisons between lidar and radiosonde over the duration of the mission. A best fit comparison of the lidar profile with the radiosonde mixing ratio is performed for each radiosonde profile. All such comparisons are then averaged to get the final calibration constant [*Ferrare et al*., 1995]. This value was 8.4 for the CAMEX2 campaign, meaning that the fully processed lidar data were multiplied by 8.4 to convert them to units of g kg^{-1}. However, averaging the calibration constants determined from the two radiosonde comparisons closest in time to the lidar data yielded a value of 8.0 or a difference of ~5%. Thus Figure 6 shows the results of retrieving droplet radius and number density for a range of maximum cloud liquid water contents using three different calibrations differing by ±5%.

In Figure 6a are shown the results using the final CAMEX2 water vapor mixing ratio calibration number of 8.4. With this calibration the retrieval technique was tested using the range of maximum cloud liquid water of 0.8–1.2 g m^{-3}. All of the retrievals in Figure 6a show the same general behavior as indicated in Figure 5. The retrieved values of droplet radius are small at the base of the cloud and rise to larger values at the top of the cloud. The number density is roughly constant through most of the lower part of the cloud and then abruptly decreases as the average radius increases. The retrieval at 0.5 km using 0.8 g m^{-3} did not converge as indicated by the zero value for retrieved radius at this altitude. Nonconvergence indicates that the input parameters are outside of the solution space of the equation. In physical terms this implies that in the lowest part of the cloud the derived liquid water content is not compatible with the lidar backscattering coefficient measured.

Figure 6b shows the results of using a value of 8.0 for the mixing ratio calibration. This amounts to a ~5% decrease in the lidar calibration constant. Using this different calibration, the level in the cloud at which supersaturation is first observed rises to ~0.55 km as compared to 0.35 km in Figure 6a. The region of the cloud between 0.35 and 0.55 km that was formerly analyzed as being supersaturated is now subsaturated, implying that there are no droplets present. Also, for the same assumed maximum liquid water as in Figure 6a the retrieved radii are smaller, and the number densities are larger. For this calibration value, no maximum liquid water content produced a roughly constant number density with height as was seen in Figure 6a. The retrievals using 0.8, 0.9, and 1.0 g m^{-3} failed to converge for the lowest altitude of the liquid water curve.

Figure 6c shows the effect of using a calibration value of 8.8, which is roughly an increase of 5% over the final CAMEX2 calibration constant. The influence of this larger calibration value is to increase the amount of supersaturation in the profile and thus the amount of liquid water retrieved. Now the portion of the cloud above 0.35 km is again supersaturated, but the retrieved particles at the base of the cloud are very large. Values range up to 50 μm depending on assumed maximum liquid water. Using this calibration, however, the retrievals converged for values of maximum liquid water down to 0.5 g m^{-3}. In general, for all of the calibrations the relationship between average radius and number density as a function of increasing maximum liquid water is the same: As the maximum liquid water is increased, the average radius increases while the number density decreases. This is to be expected since the cloud backscatter coefficient profile is the same for all of these calculations. When comparing two droplet distributions with the same backscatter coefficient, the distribution with a smaller number of larger droplets will possess the larger amount of liquid water.

Figure 6 demonstrates the difficulty of reliably measuring small amounts of liquid water scattering when this scattering is obtained in the presence of a large water vapor signal. Relatively small changes in water vapor mixing ratio calibration can

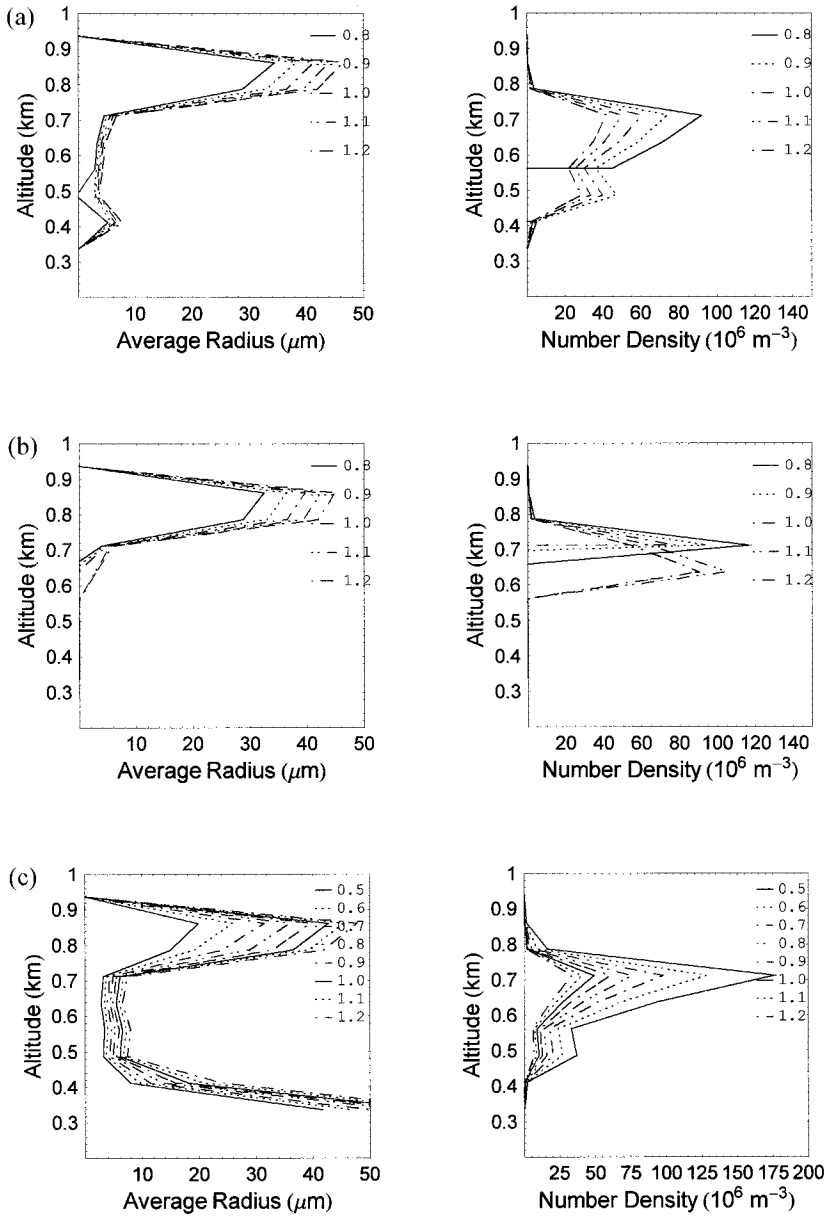

Figure 6. Sensitivity to cloud maximum liquid water content and lidar water vapor mixing ratio calibration. (a) Results based on the final water vapor calibration for the entire Second Convection and Moisture Experiment (CAMEX2). The retrievals of droplet size and number density were performed for maximum liquid water contents ranging from 0.8 to 1.2 g m^{-3}. For all of these values the retrievals in Figure 6a showed the same general relationship of droplet size tending to increase moving upward in the cloud and number density remaining roughly constant in the lower portion of the cloud and abruptly decreasing toward the top of the cloud. At 0.8 g m^{-3} the retrieval failed for the point at ~0.5 km. (b) Results based on the calibration taken just from the night of September 9, 1995, and showing the sensitivity to the water vapor calibration value. The portion of the profile in Figure 6a which indicated supersaturation and thus the presence of liquid water between about 0.35 and 0.55 km is no longer present because of the lower calibration constant. (c) The effect of increasing the calibration value to 8.8. Now quite large droplet radii are retrieved at cloud base for all values of maximum liquid water. Figure 6 demonstrates the importance of a precise calibration when measuring small amounts of liquid water in the presence of a large water vapor signal using this technique.

have a large effect on the retrieved values. Making measurements of liquid water in a portion of the Raman liquid spectrum which does not overlap the vapor would eliminate this sensitivity by allowing completely separate measurements of cloud liquid water and water vapor. This is the approach that we will follow in the future.

8.4. Other Considerations

Several additional possible influences on the calculations presented in section 8.3 will now be considered.

8.4.1. Temperature sensitivity. The influence of temperature on saturation mixing ratio and how this affects the retrieved values was mentioned in section 4. Variations in tem-

perature can affect other parameters in the calculation as well. For example, the temperature coefficient of the portion of the Raman liquid water spectrum transmitted by the water vapor filter was estimated using the laboratory data acquired at 4°C and 23°C shown in Figure 1. Between these two temperatures the temperature coefficient of this portion of the Raman band was found to be $+0.8\%\ K^{-1}$. For the data analyzed in Figure 5, the change in temperature through the cloud was <3 K, and this change in temperature is typical for the penetration depths that can be expected for the Raman technique. Thus the backscatter cross section for liquid water Raman scattering should change by less than ~2.5% under typical measurement scenarios.

Another way in which errors in temperature can affect the retrieved values is in the calculation of the aerosol backscattering coefficient. This calculation relies on a measure of density from the radiosonde which is derived from the radiosonde pressure and temperature data. The values for density are generally considered to have errors of ~2%. The sensitivity to this density variation was not tested because it will be small compared to the sensitivity to mixing ratio calibration.

8.4.2. Multiple scattering and penetration depth. Because of the fact that typical cloud droplets are large compared to the wavelength of the laser used, there is a large amount of forward scattering. This forward scattered light effectively enhances the intensity of the laser beam and tends to decrease the apparent attenuation of the beam. This greatly increases the likelihood that multiple scattering events will influence the received signals by increasing the likelihood that a given photon will undergo a scattering event that will return it to the lidar telescope. However, the input quantities required for this retrieval technique are all computed by taking ratios of signals acquired by the Raman lidar. For any such ratioed quantity, multiple scattering influences both the numerator and denominator and thus tends to cancel. For a ratio of Raman quantities such as either the water vapor or liquid water mixing ratio, the multiple scattering influence cancels almost completely [*Wandinger*, 1998]. For the aerosol backscattering ratio which involves the ratio of droplet to molecular scattering, multiple scattering introduces an error of less than ~5% [*Wandinger*, 1998].

The major effect, however, that the strong forward scattering peak has on these measurements is to allow the technique to probe more deeply into clouds. The photons that are added back into the beam by the forward scattering process are available for measurements farther into the cloud. This effect approximately doubles the penetration depth that is possible compared to the depth possible if multiple scattering were not present.

8.4.3. Differential transmission. As described in section 5, a correction must be applied in the calculation of aerosol backscattering ratio for the differential extinction that is experienced by the elastic return and the Raman-shifted nitrogen return. Such a correction is also required in the analysis of the water vapor mixing ratio. However, there is strong attenuation of the signals in the cloud, and thus it is particularly important for this correction to be applied accurately in the cloud. For the size range of droplets that populate liquid clouds and the UV laser wavelength considered here, Mie scattering coefficients are quite wavelength insensitive [*McCartney*, 1976]. (For visible wavelengths this is confirmed by the whiteness of clouds.) This implies that both the numerator and denominator of the ratios experience nearly equal extinction inside the cloud and that the ratio needs no additional differential transmission correction than that applied outside the cloud.

8.4.4. Index of refraction of cloud droplets. Cloud condensation nuclei swell to become droplets at the base of clouds, thereby introducing chemicals other than pure water into the droplet. During the swelling process the index of refraction of the aerosol changes as a function of relative humidity (RH). At 100% RH, however, regardless of the nature of the aerosol, there is a convergence of the index of refraction toward the value of pure water. Modeling work [*Shettle and Fenn*, 1979; *Runhke and Deepak*, 1984] involving various types of aerosols has shown that at 100% RH the index of refraction (at 0.55 μm) covers a range of approximately 1.33–1.36, or <3%. After the aerosol becomes a droplet and grows more in size, the index of refraction of the nucleus becomes an increasingly smaller contributor to the overall index of refraction of the droplet. Therefore the index approaches that of pure water even more closely. Because of these considerations we have used the index of refraction of pure water for the Mie scattering calculations here. In the future we will study the sensitivity of the retrievals to small variations in the assumed index of refraction.

9. Summary and Conclusions

The Raman lidar has been used to simultaneously observe Raman scattering due to liquid water and water vapor along with Mie scattering in a cloud. A retrieval technique has been developed allowing average droplet radius and droplet number density to be calculated assuming a calibration of the Raman scattering due to liquid water. The technique was shown to provide stable solutions for both average droplet radius and number density. Average droplet radius and number density were calculated from data acquired where the water vapor and liquid water signals were present in the same channel. The liquid component of the signal was obtained by subtracting the saturation mixing ratio from the combined signal. The resulting liquid water signal was then converted to liquid water content by assuming a maximum liquid water content in the cloud. The general relationship of droplets growing in size moving upward into the cloud and the number density remaining roughly constant and then abruptly decreasing near the top of the cloud was observed using the final calibration value for the CAMEX2 field campaign. Sensitivity to both mixing ratio calibration and assumed maximum liquid water content was tested showing large sensitivity to both of these parameters. An improved technique which would eliminate these sensitivities would be to measure Raman scattering from liquid water in a portion of the liquid spectrum that does not overlap the vapor signal. Such future enhancements to the Raman lidar technique should allow improved simultaneous measurements of water vapor mixing ratio, liquid water mixing ratio, and aerosol and cloud backscattering coefficient. The value of such simultaneous measurements would be to allow studies of, for instance, the relationship of aerosol and water vapor content to cloud droplet growth to be performed in regions of a cloud where existing radar-based techniques have difficulty making measurements.

Acknowledgments. We gratefully acknowledge the collaborative effort with George E. Walrafen of Howard University in Washington, D. C., which produced the Raman backscattering spectra from bulk liquid water. Thanks also go to Frank Schmidlin of NASA Goddard

Space Flight Center, Wallops Flight Facility, for the radiosonde measurements used. This work has been supported by NASA's Atmospheric Dynamics and Remote Sensing Program as well as the Department of Energy's Atmospheric Radiation Measurements program. Mention of a manufacturer's equipment does not constitute an endorsement of their products by NASA.

References

Barber, P. W., and S. C. Hill, *Light Scattering by Particles: Computational Methods*, 261 pp., World Sci., River Edge, N. J., 1990.

Bazile, R., and D. Stepowski, Measurements of the vaporization dynamics in the development zone of a burning spray by planar laser induced fluorescence and Raman scattering, *Exp. Fluids*, *16*, 171–180, 1994.

Buehler, M. F., T. M. Allen, and E. J. Davis, Microparticle Raman spectroscopy of multicomponent aerosols, *J. Colloid Interface Sci*., *146*, 79–89, 1991.

Clothiaux, E. E., T. P. Ackerman, G. G. Mace, K. P. Moran, R. T. Marchand, M. A. Miller, and B. E. Martner, Objective determination of cloud heights and radar reflectivities using a combination of active remote sensors at the ARM CART sites, *J. Appl. Meteorol*., in press, 1999.

Dong, X., T. P. Ackerman, and E. E. Clothiaux, Microphysical and radiative properties of boundary layer stratiform clouds deduced from ground-based measurements, *J. Geophys. Res*., *102*(D20), 23,829–23,843, 1997.

Ferrare, R. A., S. H. Melfi, D. N. Whiteman, K. D. Evans, F. J. Schmidlin, and D. O'C. Starr, A comparison of water vapor measurements made by Raman lidar and radiosondes, *J. Atmos. Oceanic Technol*., *12*, 1177–1195, 1995.

Goldsmith, J. E. M., F. H. Blair, S. E. Bisson, and D. D. Turner, Turn-key Raman lidar for profiling atmospheric water vapor, clouds, and aerosols, *Appl. Opt*., *37*, 4979–4990, 1998.

Guimaraes, L. G., and J. M. Nussenzveig, Uniform approximation to Mie resonances, *J. Mod. Opt*., *41*(3), 625–647, 1994.

Irvine, W. M., and J. B. Pollack, Infrared optical properties of water and ice spheres, *Icarus*, *8*, 324–360, 1968.

Khrgian, A. K. (Ed.), *Cloud Physics*, translated from Russian by Israel Program for Scientific Translation, U.S. Dep. of Comm., Washington, D. C., 1963.

McCartney, E. J., *Optics of the Atmosphere Scattering by Molecules and Particles*, 408 pp., John Wiley, New York, 1976.

Measures, R. M., *Laser Remote Sensing Fundamentals and Applications*, Wiley-Interscience, New York, 1984.

Melfi, S. H., Remote measurement of the atmosphere using Raman scattering, *Appl. Opt*., *11*, 1605–1610, 1972.

Melfi, S. H., K. D. Evans, J. Li, D. Whiteman, R. Ferrare, and G. Schwemmer, Observation of Raman scattering by cloud droplets in the atmosphere, *Appl. Opt*., *36*, 3551–3559, 1997.

Nakajima, T., M. D. King, J. D. Spinhirne, and L. F. Radke, Determination of the optical thickness and effective particle radius of clouds from reflected solar radiation measurements, part II, Marine stratocumulus observations, *J. Atmos. Sci*., *48*(5), 728–750, 1991.

Pruppacher, H. R., and J. D. Klett, *Microphysics of Clouds and Precipitation*, 954 pp., Kluwer Acad., Norwell, Mass., 1997.

Rogers, R. R., and M. K. Yau, *A Short Course in Cloud Physics*, Butterworth-Heinemann, Woburn, Mass., 1989.

Rossow, W. B., and R. A. Schiffer, Advances in understanding cloud from ISCCP, *Bull. Am. Meteorol. Soc*., *80*, 2261–2287, 1999.

Runhke, L. H., and A. Deepak (Eds.), *Hygroscopic Aerosols*, A. Deepak, Hampton, Va., 1984.

Russell, P. B., B. M. Morley, J. M. Livingston, G. W. Grams, and E. M. Patterson, Orbiting lidar simulations, 1, Aerosol and cloud measurements by an independent-wavelength technique, *Appl. Opt*., *21*, 1541–1553, 1982.

Schweiger, G., Observation of input and output structural resonances in the Raman spectrum of a single spheroidal dielectric microparticle, *Opt. Lett*., *15*(3), 156–158, 1990.

Schweiger, G., Raman scattering on microparticles: Size dependence, *J. Opt. Soc. Am. B Opt. Phys*., *8*(8), 1770–1777, 1991.

Shettle, E. P., and R. W. Fenn, Models for the aerosols of the lower atmosphere and the effects of humidity variations on their optical properties, *U.S. Air Force Geophys. Lab. Doc. AFGL-TR-79-0214*, Hanscomb Air Force Base, Mass., 1979.

Stokes, G. M., and S. E. Schwartz, The Atmospheric Radiation Measurement (ARM) Program: Programmatic background and design of the cloud and radiation testbed, *Bull. Am. Meteorol. Soc*., *75*, 1201–1221, 1994.

Vehring, R., Linear Raman spectroscopy on acqueous aerosols: Influence of nonlinear effects on detection limits, *J. Aerosol Sci*., *29*, 65–79, 1998.

Vehring, R., H. Moritz, D. Niekamp, P. Heinrich, and G. Schweiger, Linear Raman spectroscopy in droplet chains: A new experimental method for the analysis of fast transport processes and reactions on microparticles, *Appl. Spectrosc*., *49*, 1215–1224, 1995.

Vehring, R., C. L. Aardahl, G. Schweiger, and E. J. Davis, The characterization of fine particles originating from an uncharged aerosol: Size dependence and detection limits for Raman analysis, *J. Aerosol Sci*., *29*, 1045–1061, 1998.

Wandinger, U., Multiple-scattering influence on extinction- and backscatter-coefficient measurements with Raman and high-spectral-resolution lidars, *Appl. Opt*., *37*, 417–427, 1998.

Whiteman, D. N., S. H. Melfi, and R. A. Ferrare, Raman lidar system for the measurement of water vapor and aerosols in the Earth's atmosphere, *Appl. Opt*., *31*, 3068–3082, 1992.

Whiteman, D. N., W. F. Murphy, N. W. Walsh, and K. D. Evans, Temperature sensitivity of an atmospheric Raman lidar system based on a XeF excimer laser, *Opt. Lett*., *18*(3), 247–249, 1993.

Whiteman, D. N., G. E. Walrafen, W.-H. Yang, and S. H. Melfi, Measurement of an isosbestic point in the Raman spectrum of liquid water by use of a backscattering geometry, *Appl. Opt*., *38*, 2614–2615, 1999.

Wiscombe, W. J., R. M. Welch, and W. D. Hall, The effects of very large drops on cloud absorption, part I, Parcel models, *J. Atmos. Sci*., *41*(8), 1336–1355, 1984.

S. H. Melfi, Department of Physics, University of Maryland, Baltimore County, Baltimore, MD 21250.

D. N. Whiteman, Laser Remote Sensing Branch, NASA Goddard Space Flight Center, Greenbelt, MD 20771. (david.whiteman@gsfc.nasa.gov)

(Received May 26, 1999; revised August 25, 1999;
accepted September 14, 1999.)